

HEMATOPOIESIS AND STEM CELLS

Decoding functional hematopoietic progenitor cells in the adult human lung

Catharina Conrad,¹ Mélia Magnen,¹ Jessica Tsui,² Harrison Wismer,² Mohammad Naser,² Urmila Venkataramani,² Bushra Samad,² Simon J. Cleary,¹ Longhui Qiu,¹ Jennifer J. Tian,¹ Marco De Giovanni,³ Nicole Mende,⁴ Andrew D. Leavitt,¹ Emmanuelle Passegué,⁵ Elisa Laurenti,⁴ Alexis J. Combes,^{1,2,6-8} and Mark R. Looney^{1,7-9}

¹Department of Medicine, ²UCSF CoLabs, and ³Department of Microbiology and Immunology, University of California San Francisco, San Francisco, CA; ⁴Wellcome-MRC Cambridge Stem Cell Institute, Department of Hematology, University of Cambridge, Cambridge, United Kingdom; ⁵Columbia Stem Cell Initiative, Columbia University Irving Medical Center, New York, NY; and ⁶Department of Pathology, ⁷Bakar ImmunoX Initiative, ⁸Biomedical Sciences Program, and ⁹Department of Laboratory Medicine, University of California San Francisco, San Francisco, CA

KEY POINTS

- **Functional hematopoietic stem cells with unique gene signatures reside in the adult human lung.**
- **These cells contribute to the pool of hematopoietic stem cells mobilized for stem cell transplantation.**

Although the bone marrow is the main site of blood cell production in adults, rare pools of hematopoietic stem and progenitor cells have been found in extramedullary organs. In mice, we have previously shown that the lung contains hematopoietic progenitor cells and is a site of platelet production. Here, in the adult human lung, we show that functional hematopoietic precursors reside in the extravascular spaces with a frequency similar to the bone marrow and are capable of proliferation and engraftment in mice. The gene signature of pulmonary and medullary CD34⁺ hematopoietic progenitors indicates greater baseline activation of immune-, megakaryocyte/platelet-, and erythroid-related pathways in lung progenitors. Spatial transcriptomics mapped blood progenitors in the lung to an alveolar interstitium niche with only a few cells identified in an intravascular location. In human blood samples collected for stem cell transplantation, CD34⁺ cells with a lung signature enriched the mobilized pool of hematopoietic stem cells. These results

identify the lung as a pool for uniquely programmed blood stem and progenitor cells with the potential to support hematopoiesis in humans.

Introduction

Hematopoietic stem cells (HSCs) are self-renewing cells residing in the bone marrow (BM) that are ultimately responsible for production of all mature circulating blood cell lineages.¹ Despite the burden of maintaining hematopoiesis, HSCs are a rare cell type in the BM accounting for <0.01% of nucleated cells.^{2,3} They occupy and are maintained by a specific BM niche yet are able to exit the BM environment and enter the circulation, although the explanation of this behavior is largely unknown.⁴ HSCs are central to the pathogenesis of serious disorders including myelodysplasia, acute and chronic leukemia, aplastic anemia,⁵ and clonal hematopoiesis,⁶ and HSC transplantation can be a lifesaving therapy. Previously, we identified a population of hematopoietic stem and progenitor cells (HSPCs) in the mouse lung, but their function was unclear.⁷ Motivated by this background, in this study we sought to determine whether HSPCs occupied the adult human lung, an organ with a vast vasculature that contains a wide-ranging repertoire of stromal and immune cells, and to determine the niche and function of these cells.

Methods

Human samples

Fresh human tissues were obtained from deceased organ donors after either brain death or circulatory death (supplemental Table 1, available on the *Blood* website). All patients were on mechanical ventilation and treated in the intensive care unit until organ retrieval. Lungs and vertebral bodies were surgically recovered and immediately placed on ice. Peripheral blood (PB) was collected in sodium heparin tubes. Healthy human stem cell donors were treated with a granulocyte colony-stimulating factor mobilization regimen, and PB stem cells were collected by apheresis. We received 1 mL of the mononuclear fraction that would have otherwise been discarded. Isolation of cells, magnetic enrichment, antibody staining, cell sorting, and immune phenotyping by flow cytometry are described in the supplemental Methods.

Cell culture assays

Lineage depleted BM or lung cells were plated in MethoCult or MegaCult-C medium according to the manufacturer's

instructions. After incubation for 10 to 14 days at 37°C in 5% CO₂, hematopoietic colonies were scored based on morphologic and phenotypic criteria and quantified by manual counting using brightfield microscopy. Further details are described in the supplemental Methods.

Xenotransplantation

NSG-SGM3 mice (NOD.Cg-Prkdc^{scid} Il2rg^{tm1Wjl} Tg[CMV-IL3, CSF2, KITLG]1Eav/MloySzJ, Stock No: 013062) were purchased at the Jackson Laboratory and housed in a specific pathogen-free animal facility. One day before reconstitution, mice were preconditioned by sublethal irradiation (2.4 Gy).⁸ On the day of transplantation, lineage-negative (Lin⁻) lung and BM cells were thawed and 1.5 × 10⁶ viable cells were IV injected into the tail vein of recipient mice.⁸ Matched lung and BM cells were transplanted into recipient mice where possible. Ten weeks after transplantation, the BM, lung, and blood were investigated for engraftment of human cells. Further details are described in the supplemental Methods.

scRNA-seq

Live, Lin⁻ CD34⁺ cells from the lung and BM were sorted for subsequent 10× Genomics single-cell RNA sequencing (scRNA-seq). Live, Lin⁺ cells were collected for demultiplexing the samples from different individuals based on single nucleotide polymorphisms.⁹ Further details of scRNA-seq workflow and the bioinformatic analysis are provided in the supplemental Methods.

Spatial transcriptomics

Human lung tissue from deceased organ donor samples was frozen in optimal cutting temperature on dry ice, and tissue blocks were processed at the facility of Resolve Biosciences, San Jose, for spatial transcriptomics using a custom 100 gene panel. Further details on spatial transcriptomics workflow and the bioinformatic analysis are provided in the supplemental Methods.

Statistical analysis

Statistical analysis was done with GraphPad Prism version 10.0.2, R/RStudio version 4.0.3, or Python version 3.12.1. Statistics for each analysis are described in the relevant section.

Our study does not involve human subjects because the tissue involved was obtained from deceased research donors or from samples obtained during routine clinical collections from apheresis stem cell donors that would have been otherwise discarded. The mouse xenotransplantation experiments were performed under the University of California San Francisco Institutional Animal Care and Use Committee approval (AN201629).

Results

The adult human lung contains functional HSPCs

We had the unique opportunity to receive matched adult human lungs, vertebral bodies (BM), and PB freshly recovered from deceased research donors (supplemental Table 1). The lungs were extensively perfused at the time of collection, and we selected healthy-appearing lung tissue for experiments (supplemental Figure 1A). After tissue dissociation and the

rendering of single-cell suspensions, we characterized live, Lin⁻ cells (Figure 1A) using standard surface markers for HSPCs (supplemental Table 2).¹⁰⁻¹² Notably, our lineage panel contained markers for mature immune, endothelial, and epithelial cells, allowing for the phenotyping of rare Lin⁻ CD34⁺ cells. We discovered a distinct population of multipotent (MP) cells (CD34⁺/CD38⁻) in the lung and BM and very few of these cells in the PB (Figure 1B). The lung and BM contained cells with surface staining consistent with HSCs (CD34⁺/CD38⁻/CD90⁺/CD45A⁻) but these cells were absent in the PB. Multipotent progenitor (MPP) cells (CD34⁺/CD38⁻/CD90⁻/CD45A⁻) were observed in all 3 tissues. More committed hematopoietic progenitor cells (HPCs; CD34⁺, CD38⁺), such as common myeloid progenitor (CMP; CD34⁺/CD38⁺/CD45A⁻/Flt-3⁺), granulocyte-macrophage progenitor (GMP; CD34⁺/CD38⁺/CD45A⁺/Flt-3⁺), and megakaryocyte-erythroid progenitor cells (MEP; CD34⁺/CD38⁺/CD45A⁻/Flt-3⁻) were observed in all 3 tissues but were less common in the lung (Figure 1B-C). Overall, the BM and PB had nearly identical proportions of hematopoietic progenitors, whereas Lin⁻ lung cells were enriched for immunophenotypic HSCs and MPPs (Figure 1C-D).

To rule out residual blood as a source of HSPCs in perfused lungs, we estimated the numbers of progenitors in equivalent volumes of blood and lung tissue, yielding lung HSPC numbers that could not be explained by retention of intravascular blood in lungs (supplemental Figure 1B). Furthermore, the distinct proportions of cell subsets in the lung and blood indicate a tissue-specific progenitor composition. Remarkably, the frequency of the immunophenotypic MP pool in the lung is similar to the BM (Figure 1E), whereas the pool of more committed hematopoietic progenitor cells (HPCs) is much smaller in the lung (Figure 1E). We also tested for the effects of donor age and sex on our results and found that increasing age was associated with fewer numbers of HSPCs in the BM but not in the lung (supplemental Figure 1C). Sex was not associated with changes in HSPC frequency in the BM or lung (supplemental Figure 1D).

Given that fibroblasts are generally Lin⁻ cells, but some can be CD34 positive,¹³ we included a marker for fibroblasts (platelet-derived growth factor receptor α [PDGFRA]) in our lineage panel to determine whether fibroblast contamination could affect our results, but we did not detect any changes in HSPC frequencies between our 2 lineage panels (supplemental Figure 2A-C).

We next tested the functional capacity of lung HSPCs using in vitro colony-forming assays. We plated Lin⁻ cells from the lung or BM in MethoCult and observed a variety of colonies from both tissues. The Lin⁻ cells from the lung produced overall fewer colonies, but with a significant increase in the relative proportion of erythroid colonies (burst-forming unit erythroid [BFU-E]; Figure 1F; supplemental Figure 3A). After morphologic colony assessment, we used flow cytometry (supplemental Figure 3B-D) to confirm cellular colony composition and found that lung colonies were enriched with cells expressing the erythrocyte marker GlyA (supplemental Figure 3D). There were not enough Lin⁻ cells from the PB to perform a comparative study, so we determined the colony-forming unit (CFU) potential of nucleated blood cells. This yielded few colonies (supplemental Figure 3E-G), including only a few BFU-E colonies, which is the predominant colony type produced by the

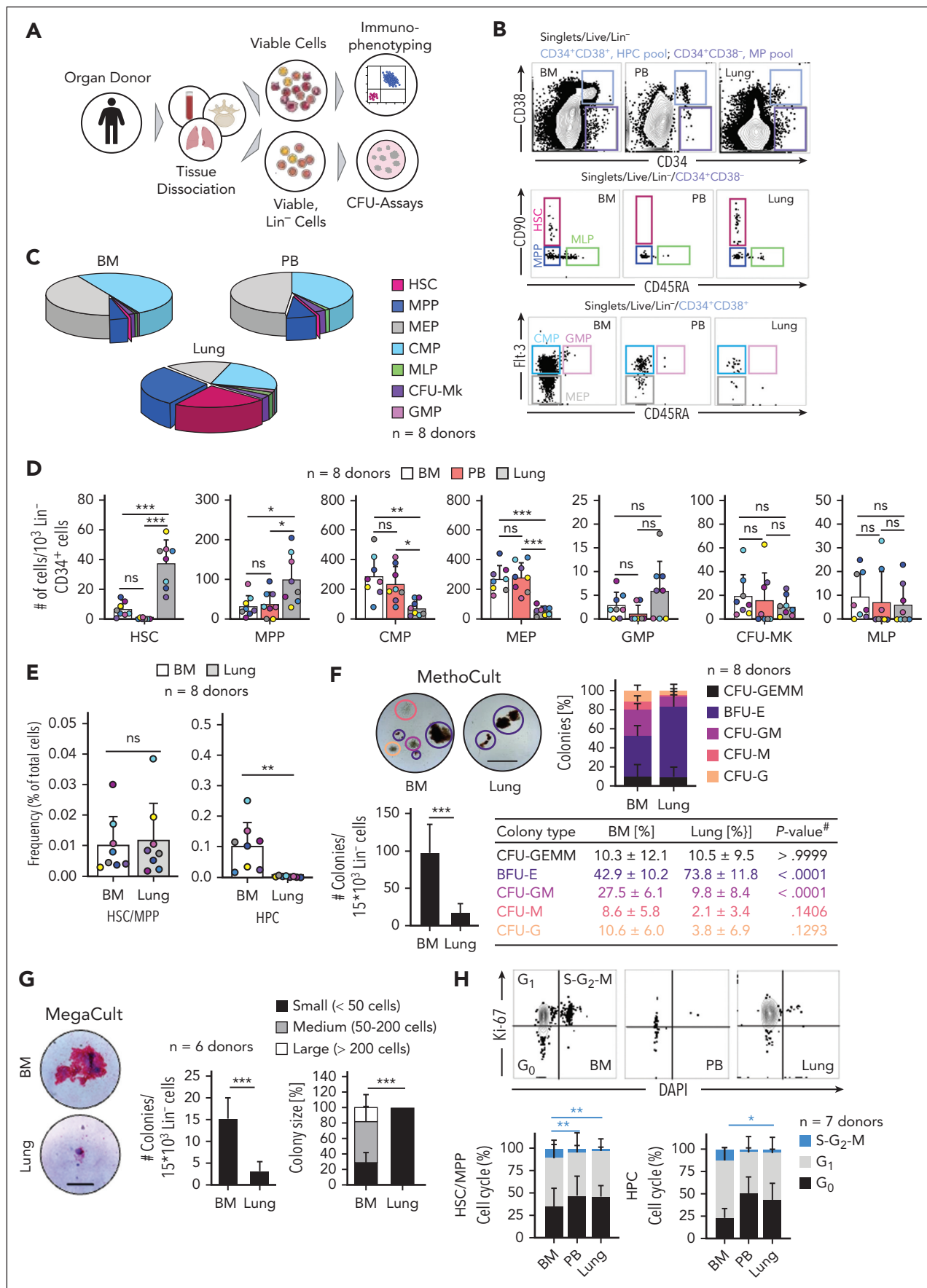


Figure 1.

lung. These results strengthen our conclusion that the presence of lung HSPCs is not an artifact of blood contamination. We also plated Lin^- cells in MegaCult to test the potential to produce megakaryocytes, a cell population that we previously described as resident cells in the mouse lung.⁷ Both BM and lung cells were capable of producing megakaryocyte colonies although the lung produced fewer and small colonies (Figure 1F). In addition, we sorted lung and BM HSCs and HPCs into MegaCult and observed that lung HSCs produced comparatively more megakaryocytes (supplemental Figure 4A), whereas in BM most cells with CFU megakaryocyte capacity are derived from precursors in the HPC fraction (supplemental Figure 4B).

Overall, the fewer colonies observed from lung cells may also relate to reduced cell cycling compared with the BM (Figure 1H). The molecular cues that regulate the transition to activity in pulmonary HSPCs are not known and could be different from growth factors added in classical in vitro CFU assays. Together, we conclude that the human lung contains functional HSPCs that exhibit a bias toward erythroid and megakaryocyte lineages within the hematopoietic progenitor tree.

Human lung-derived hematopoietic progenitors have engraftment potential

We next tested whether HSPCs isolated from the lung are capable of engraftment when xenotransplanted into immunodeficient mice.⁸ We chose NSG-SGM3 mice (human stem cell factor, granulocyte-macrophage colony-stimulating factor, interleukin-3) to support human myeloid cell engraftment¹⁴ for these experiments in which we adoptively transferred magnetic-enriched Lin^- cells from the lung or BM into mice after sublethal irradiation.¹⁵ Given that the production of erythroid cells in xenograft models is not reliable owing to the lack of cross-reactivity between mouse erythropoietin (EPO) and the human EPO receptor, mice received recombinant human EPO injections in the final 3 weeks of the experiment (Figure 2A) as described previously.⁸ Human cells in the BM, lung, and PB of recipient mice were assessed after 10 weeks, a time point that is commonly used to measure human HSC activity in vivo.¹⁵⁻¹⁷ Engraftment was rigorously defined as the presence of human CD45^+ cells, using 2 different antibody clones, with the threshold for engraftment set to $\geq 0.01\%$ CD45^{++} cells of all CD45^+ cells (mouse and human) with at least 30 cells recorded in the CD45^{++} gate for BM and lung, and ≥ 15 cells for PB⁸ given that low levels of engrafted human cells are expected from previous studies.¹⁷ Examples of positive and negative engraftment (sublethal irradiation without adoptive cell transfer) are

shown in Figure 2B. Overall, 6 of 7 mice with BM-derived HSPCs and 5 of 7 mice with lung-derived HSPCs engrafted in the BM and in the lung tissue (Figure 2C; supplemental Figure 5A). In the PB, engraftment was observed in 4 of 7 mice with BM-derived HSPCs and 2 of 7 mice with lung-derived HSPCs (Figure 2C; supplemental Figure 5A). Examples of BM- or lung-derived cells in the mouse BM or lung are shown in Figure 2D.

We also determined erythroid engraftment using the gating strategy in Figure 2E to detect CD45^- , human GlyA^+ , and human CD71^+ cells and observed similar erythroid engraftment of BM- or lung-derived HSPCs in the mouse BM, lung, or PB (Figure 2F-G; supplemental Figure 5B). Similar to BM-derived HSPCs, lung-derived HSPCs were capable of multilineage blood cell production (Figure 2H; supplemental Figure 5C-E).

Human lung HSPCs have unique transcriptional programming

The availability of matched lung and medullary HSPCs allowed us to directly compare their transcriptional profiles using scRNA-seq (supplemental Figure 6A). Our gating strategy is shown in supplemental Figure 6B-C. We integrated all samples using Harmony¹⁸ and generated a batch-corrected uniform manifold approximation and projection (UMAP) to identify clusters of transcriptionally similar cells. We filtered out stromal and mesothelial cell populations and subsetted progenitor cells (supplemental Figure 6C-E). Using the function "findConservedMarkers," we identified genes that were consistently expressed across BM- and lung-derived cells and annotated clusters based on a reference data set.^{19,20} Dimensionality reduction yielded a visual representation consistent with HSC and MPP production of progenies with progressive commitment to more differentiated fates (Figure 3A; supplemental Figure 6F-G). To validate our annotation, we generated coregulated modules of differentially expressed genes using Monocle3.²¹ The module highly specific for HSCs contains genes such as *AVP*, *SPINK2*, *SELL*, and *HOPX* and was strongly expressed in cells from both the BM and lung (Figure 3B; supplemental Figure 7A-B). We ordered the cells along a pseudotime trajectory to reconstruct their developmental path for each tissue individually, suggesting a relationship between HSCs and stromal cells in the lung that was absent in cells derived from the BM (Figure 3C). As previously discussed, some pulmonary fibroblasts are CD34^+ , and these results could point to the ontogeny of a subset of lung stromal cells.

Figure 1. The human lung contains phenotypic hematopoietic progenitors with in vitro proliferation and differentiation capacity. (A) Pipeline for flow-cytometric immunophenotyping and evaluation of in vitro colony-forming capacity of progenitors from BM, lung, and PB of organ donors. (B) Normalized flow cytometry plots of BM and PB in the Live/Lin^- gate from a representative donor showing stem cell subsets within the multipotent (MP [$\text{CD34}^+\text{CD38}^-$], light purple) and the hematopoietic progenitor cell (HPC [$\text{CD34}^+\text{CD38}^+$], light blue) pool. (C) Composition of hematopoietic progenitor subsets in the BM, PB, and lung ($n = 8$). (D) Numbers of HPC subsets in the BM (white), PB (red), and lung (gray) per $10^3 \text{Lin}^- \text{CD34}^+$ cells. $N = 8$ donors; bars indicate mean number of cells \pm standard deviation (SD), and colors of the dots represent individual donors. Analysis of variance (ANOVA) followed by Sidak multiple comparison test, $*P < .03$; $**P < .002$; $***P < .0001$. (E) Frequency of HSCs/MPPs and HPCs as a percentage of total nucleated cells in the lung or BM, respectively. Dot colors represent individual donors, bars indicate mean \pm SD. Student t test, $**P < .01$. (F) Culture-initiating capacity of lung and BM progenitors in MethoCult ($n = 8$): representative colonies (scale bar, 500 μm), colony composition, and colony quantity for progenitors derived from the BM and lung. Student t test, $***P < .0001$. #ANOVA followed by Sidak multiple comparison test. BFU-E (purple), burst-forming unit erythroid; G (orange), granulocyte; M (red), macrophage; GM (pink), granulocyte macrophage; GEMM (black), granulocyte, erythroid, macrophage, and megakaryocyte. (G) Culture-initiating capacity of lung and BM progenitors in MegaCult ($n = 6$): representative colonies (scale bar, 100 μm), colony quantity, and colony size for progenitors from the BM and lung. Bar graph represents mean number of colonies \pm SD, Student t test, $***P < .0001$. Stacked bars represent mean proportion \pm SD, Kruskal-Wallis test, $***P < .0001$. (H) Proportions of cycling (S-G2-M phase [blue], Ki-67 $^+$ DAPI $^+$), preparing/growing (G1 [gray], Ki-67 $^+$ DAPI $^-$), and resting cells (G0 [black], Ki-67 $^-$ DAPI $^-$) in the HSC/MPP and HPC pool from BM, PB, and lung ($n = 7$). Stacked bars represent mean proportion \pm SD, ANOVA followed by Sidak multiple comparison test, $**P < .01$, $*P < .05$. For comparisons not indicated, no statistically significant differences were observed. CFU-Mk, CFU megakaryocyte; CMP, common myeloid progenitor; DAPI, 4',6-diamidino-2-phenylindole; GMP, granulocyte-macrophage progenitor; MEP, megakaryocyte-erythroid progenitor; MLP, multilymphoid progenitor; ns, not significant.

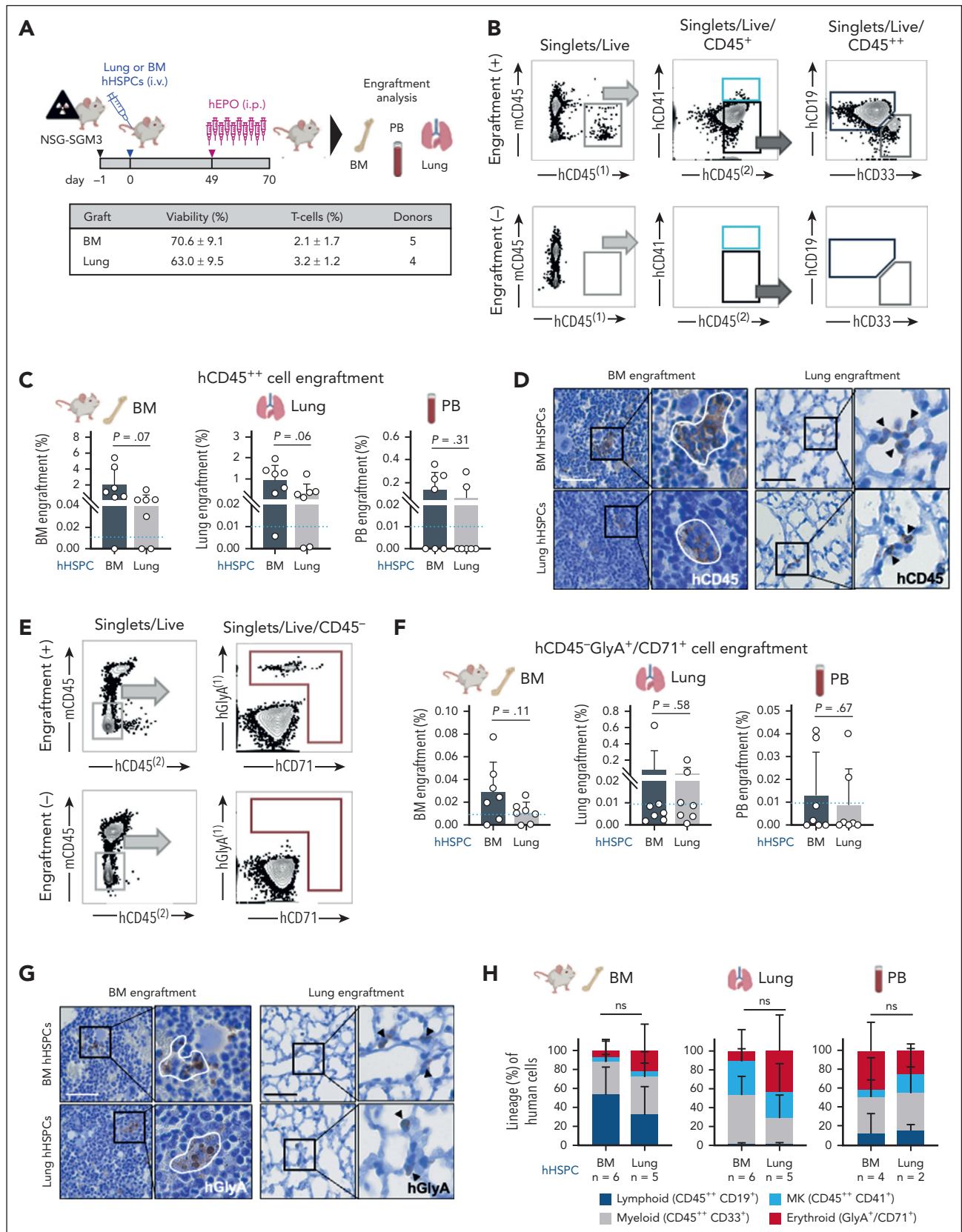


Figure 2. Human lung-derived hematopoietic progenitors have in vivo engraftment potential. (A) Experimental procedure to compare the in vivo engraftment efficiency of lung and BM hematopoietic progenitors: after sublethal irradiation, NSG-SGM3 mice were injected IV with either 1.5×10^6 Live/Lin⁻ human lung or BM cells. Ten weeks after transplantation, the BM, PB, and lung of recipient mice were collected and investigated for human cell engraftment. The graft properties are summarized in the table below. (B) Representative flow plots of human myeloid (hCD45⁺, hCD33⁺) and lymphoid (hCD45⁺, hCD19⁺) cell engraftment in the BM of a recipient mouse (+, upper panel)

Next, we compared the differential gene expression between medullary and lung cells within the HSC/MPP cluster and plotted the median expression of both cells on a scatterplot (Figure 3D). Using the Wilcoxon rank-sum test in Seurat's "FindMarkers," we identified 50 genes that were upregulated in lung HSCs and 10 genes that were higher in BM cells (Figure 3D). Among the top upregulated genes in lung HSCs, several genes (*CEBPB*, *SOD2*, *PLCG2*, *HSPA1A*) were associated with maintaining HSC quiescence and fitness (Figure 3E).²²⁻²⁵ We attributed the highest biological relevance to genes that were upregulated in most of the cells, as validated by analyzing the distribution of gene expression values (Figure 3F-H). HSCs from the lung have unique features (Figure 3F) and share characteristics of the hematopoietic lineage (Figure 3G), whereas, as expected, cells from the BM have a high expression of classical stem cell genes (Figure 3H).¹⁹

Next, we performed single-sample gene set enrichment analysis to identify pathways that are differentially regulated between cells from the lung and the BM. The enrichment scores were calculated across all individual cells and tissues for gene set collections from the Molecular Signature Database (H, hallmark; CP, canonical pathways; C5, ontology). In the gene sets analyzed, repeatedly pathways associated with EPO signaling, platelet function, and immune responses were found to be upregulated in pulmonary HSCs (Figure 3I). Side-by-side comparison of selected pathways indicates that HSCs from the lung are enriched for megakaryocyte (R-HSA-8936459) and EPO-induced erythroblast (R-HSA-9027277, R-HSA-9006335) differentiation, as indicated by higher normalized enrichment scores (Figure 3J). Our finding of increased EPO signaling pathways in lung HSCs is consistent with our data in Figure 1E on the erythroid-biasing of lung colonies. Our finding of platelet and megakaryocyte-skewing of lung HSCs is provocative in light of previous work on platelet production in the lung and tissue-resident immune-like megakaryocytes.^{7,26,27} In addition, we found inflammatory signaling to be upregulated in pulmonary HSCs (Figure 3K), suggesting that these cells could impart unique immunological functions of their progeny.

A small cluster of cells has recently been suggested as an HSC population in an analysis of the healthy and diseased human lung tissue based on *CD34*, *SPINK2*, *STMN*, and *PRSS57* expression,²⁸ but the self-renewal and differentiation potential and the location of these cells are not known. In addition, *CD34*⁺ cells can be found in endothelial, lymphatic, and fibroblast clusters (supplemental Figure 8A-B). To identify potential HSCs based on their transcriptomic profile, we used UCell scoring to find *Lin*⁻ *CD34*⁺ cells with an HSC signature in a data set combining 9 human lung scRNA-seq studies (Human Lung Cell Atlas V2²⁹; supplemental Figure 8C-D). We projected these

cells on our UMAP structure of HSPCs from the lung and BM (Figure 3A) in supplemental Figure 8E and mapped 43 cells to the HSC/MPP cluster (supplemental Figure 8F) across all integrated data sets in the Human Lung Cell Atlas (supplemental Figure 8G). We conclude that, given their rarity and the coexpression of *CD34* in multiple lung cell types, lung HSCs are mostly masked and overlooked when using standard unsupervised clustering techniques.

HSPCs in the lung reside in the extravascular tissue

The lung is composed of diverse cell entities, such as epithelial, endothelial, stromal, and immune cell subpopulations that could provide a unique niche for HSPC maintenance and differentiation.²⁰ We used immunostaining to localize putative HSCs (*Lin*⁻/*CD34*⁺/*CD90*⁺) in human lung and BM and found HSCs that localized to the alveolar interstitium (Figure 4A; supplemental Figure 9A-B). To characterize the pulmonary HSC niche, we used a spatial transcriptomics approach based on combinatorial single-molecule fluorescence in situ hybridization (Figure 4B). We designed a marker panel that characterizes HSPCs and the common cell entities of the lung (supplemental Table 3). After QuPath-based cell segmentation, we annotated the lung cells by performing unsupervised clustering on transcript expression values (Figure 4C; workflow shown in supplemental Figure 10A-D). We filtered for putative HSPCs defined by *CD34*⁺ positivity, expression of HSPC-associated transcripts, and negativity for marker genes of other lung cell entities (Figure 4C; workflow shown in supplemental Figure 10E-F; supplemental Figure 11A-B). We visually validated all candidate cells and assigned them to their anatomic location. More than 90% of cells matching the criteria for HSPCs localized to the extravascular lung, with most cells in the alveolar interstitium or in proximity of bronchi (peribronchial) and vasculature (perivascular) (Figure 4D; supplemental Figure 11A). To define the neighborhood of HSPCs on the cellular level, we used Squidpy for co-occurrence analysis across all samples³⁰ suggesting that the immediate HSPC niche is mainly formed by endothelial cells, although epithelium and fibroblasts have a steady presence (Figure 4E-F; supplemental Figure 11C).

HSCs with pulmonary signatures are mobilized during apheresis collections for stem cell transplantation

Finally, we evaluated the potential function of pulmonary HSCs by evaluating their contribution to the mobilized blood progenitor pool. In 8 healthy volunteers undergoing mobilized blood donations for stem cell transplantation (apheresis donations), we analyzed the transcriptomic profile of *Live/Lin*⁻/*CD34*⁺ cells by scRNA-seq (Figure 5A-B). After cell annotation (Figure 5C), we subsetted the HSCs per donor (Figure 5D) and calculated tissue-specific signature scores using UCell to infer

Figure 2 (continued) and nontransplanted control (-, lower panel). (C) Engraftment efficiency of human cells after xenotransplantation measured by flow cytometry. Bar graphs represent the percentage of *hCD45*⁺ cell engraftment in the BM, lung, and PB of recipient mice after transplantation of HSPCs from human BM (black) or lung (white). Mean ± SD; Student t test values are given, and individual data points for each animal are plotted as gray dots. Blue dotted line indicates threshold for positive engraftment. (D) Detection of human cells in the BM (left panel) and lung (right panel) of recipient mice by immunostaining against human *CD45* (*hCD45*). Scale bar, 50 μm. (E) Representative flow cytometry plots of human erythroid (*CD45*⁻, *hGlyA*⁺, or *hCD71*⁺) cell engraftment in the BM of a recipient mouse (+, upper panel) and nontransplanted control (-, lower panel). (F) Human erythroid cell expansion (*CD45*⁻, *hGlyA*⁺, or *hCD71*⁺) in the BM, lung, and PB of recipient mice measured by flow cytometry. Bar graphs representing the percentage of *CD45*⁻*hGlyA*⁺*hCD71*⁺ cells in BM, lung, and PB after transplantation of HSPCs from human BM (black) or lung (white). Mean ± SD; Student t test values are given, and individual data points for each animal are plotted as gray dots. Blue dotted line indicates threshold for positive engraftment. (G) Detection of human erythroid cells in the BM (left panel) and lung (right panel) of recipient mice by immunostaining against human *GlyA* (*hGlyA*). Scale bar, 50 μm. (H) Proportion of lineage expansion across all human cells detected in the BM, lung, and PB, respectively. Stacked bars represent mean proportion ± SD; ANOVA followed by Sidak multiple comparison test; ns, not significant.

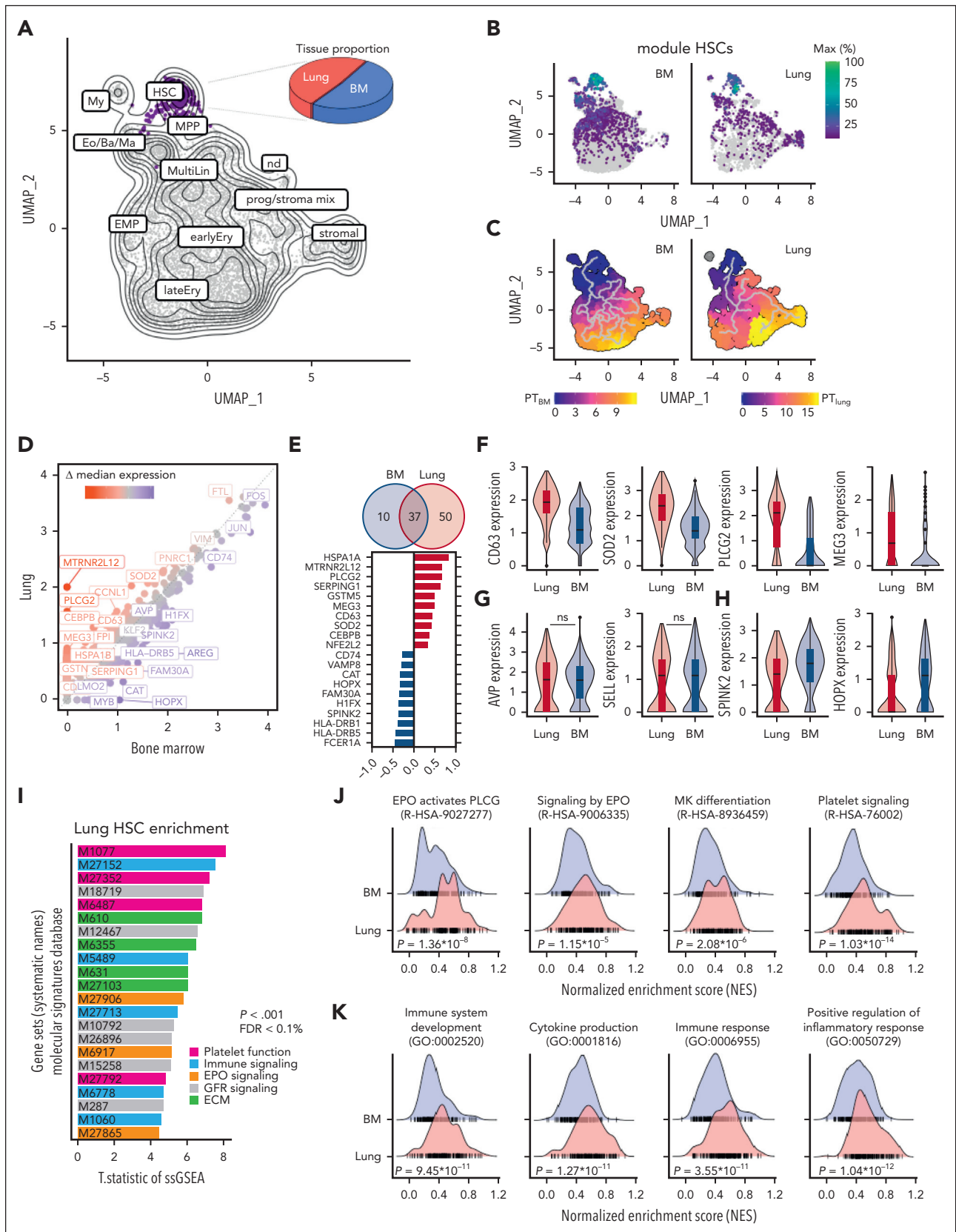


Figure 3. Comparative transcriptomic analysis of lung and BM HSCs reveals shared and unique gene expression profiles. (A) Uniform manifold approximation and projection (UMAP) projection of BM and lung Lin⁻ CD34⁺ progenitor hierarchy from 8 human donors highlighting the HSC/MPP cluster (purple). The pie graph indicates the proportion of cells from the BM (blue) and lung (red) within the MP subset. (B) Grouping of gene expression patterns into modules using Monocle3. Aggregate expression values of genes in the module highly specific for HSCs (supplemental Figure 7) are shown individually for the BM and lung. (C) Pseudotime calculation for each cell within the

their source (supplemental Table 4). We determined that ~25% of mobilized HSCs were of extramedullary origin including ~15% of total cells being of pulmonary origin (Figure 5E-G). These results indicate that extramedullary HSCs are mobilized into the HSC pool used for transplantation and points to their potential biological function.

Discussion

For many years, HSCs were viewed as unbiased cells that initiated hematopoietic development and specialization. Enabled by new technologies, our understanding of hematopoiesis has been refined to include the possibility that developmental biases may be present even in these most undifferentiated cells, such as with megakaryocyte-biased HSCs.¹¹ However, the mechanisms responsible for this early biasing or specialization are not clear.^{31,32} Here, we propose that the traditional view of HSC residency in the BM should be reconsidered to include extramedullary tissues, such as the lung. Indeed, and remarkably, we found an equal frequency of multipotent cells residing in the BM and lung. Owing to the low frequency, we used approaches to enrich for the presence of HSPCs in our studies, which were not done in previous studies and likely enabled the profiling of this rare subset of cells among the >30 different lung cell types.

It is clear from our studies that the lung HSPCs have unique features compared with their medullary counterparts, but also to HSPCs found at other extramedullary sites (PB and spleen³³). Chief among these, and perhaps obvious from our understanding of lung biology, is that lung HSPCs, like spleen HSPCs, are less active in terms of cell division and the production of more differentiated and specialized hematopoietic cells than their BM counterparts.³³ These results from *in vitro* experiments would suggest that lung HSPCs function as a reserve pool that could be mobilized in the setting of hematopoietic stress or, as we have shown here, during stem cell collections for transplantation. Further studies are needed to define physiological and pathological stimuli that trigger hematopoiesis in the lung.

Our xenotransplantation experiments indicated that lung HSPCs performed similarly to medullary HSPCs, when given the challenge of engraftment after sublethal irradiation. A wide range of engraftment levels and analysis time points have been used for measuring human HSC activity *in vivo*, and there is no standard in the field.¹⁷ Thus, despite low graft expansion in our model (NSG-SGM3 mice, sublethal irradiation, IV HSPCs), our data are consistent with previous outcomes and demonstrate self-renewal capacity of pulmonary HSPCs

in vivo. In addition, we included donors of any age and sex (supplemental Table 1), which might have contributed to larger variations in our results.

Our transcriptomics analysis revealed a distinct molecular program in lung HSPCs that was further distinguishing compared with medullary HSPCs. We found clear megakaryocyte biasing of lung vs medullary HSPCs indicating that perhaps the lung is a source of these biased progenitors. Our colony analysis of lung HSCs also supports megakaryocyte biasing. This is an intriguing finding given (1) the role of the lung in platelet biogenesis⁷ and (2) the presence of tissue-resident immune-like megakaryocytes in the lung that may be derived from a lung progenitor.^{26,27} We further found an erythroid bias of lung HSPCs, akin to that reported in PB and spleen HSPCs.³³ Therefore, erythroid bias is a shared feature of steady-state extramedullary HSPCs, perhaps determined by distinct access to environmental oxygen vs the relatively hypoxic environment of the BM.³⁴

Our immunofluorescence imaging and spatial transcriptomic studies were essential in confirming the presence of HSPCs in the lung and defining their precise locations and niche. Given the prevailing dogma that hematopoietic precursors widely circulate,³⁵⁻³⁷ it was important to rule out that blood contamination was producing our results. We found a few intravascular HSPCs, confirming previous studies, but most were extravascular and predominately in vascular-rich zones of the lung alveoli. This anatomic location in the lung is similar to the location of HSPCs in the BM, which are closely positioned next to the vascular sinusoids.^{38,39} In the lung, this positioning could be important for seeding of the lung with circulating HSCs and potentially for exiting the lung during hematopoietic stress or during mobilization for stem cell collections. In this niche, it was notable that lung fibroblasts were in close proximity. The lung mesenchyme is well known to be a critical niche supporting epithelial cell development and repair and similar mechanisms could be operable influencing lung HSPCs.^{40,41} In addition, we identified a developmental trajectory between lung HSPCs and lung stromal cells. Subpopulations of lung fibroblasts are known to be CD34⁺, and previous lineage-tracing experiments in pulmonary fibrosis have shown a hematopoietic contribution to fibroblasts.^{42,43} Future studies are needed in this area to understand how lung HSPCs could be involved in fibrotic lung diseases.

Our study does have limitations. We used human deceased donors for tissue collection, and there may be biases introduced in the mechanisms of their deaths and how that influences HSC biology. There is also donor heterogeneity,

Figure 3 (continued) BM and lung using Monocle3 to infer progression through different cellular differentiation to provide insights into the developmental trajectory. (D) Scatterplot of median gene expression of cells in the HSC/MPP cluster from the lung (red) and BM (blue) to visualize consistent (gray) and differentially (highlighted) expressed genes. (E) Venn diagram and top 10 differentially expressed genes. The number in each circle represents the amount of differentially expressed genes between lung (red) and BM (blue), and the overlapping number indicates mutual differentially expressed genes based on the Wilcoxon rank-sum test in Seurat's "FindMarkers" function. (F) Box and violin plots showing the distribution of selected genes upregulated in pulmonary HSCs. Wilcoxon adjusted $P < .001$. (G) Selection of marker genes shared between lung and BM as box and violin plots, respectively. (H) Box and violin plots showing the distribution of markers genes upregulated in BM HSCs, Wilcoxon adjusted $P < .001$. (I) T-statistic of single-sample gene set enrichment analysis (ssGSEA) scores for selected gene sets (Hallmark, Reactome, Biocarta, KEGG) enriched in pulmonary HSCs categorized by recurring functions. (J) Enrichment ridge plots comparing the distribution of enrichment scores in HSCs from lung (red) and BM (blue) of selected Reactome pathways. Rug plots indicate the scores of individual cells along the ridge plot. P values are given in the figure, FDR R-HSA-9027277 = 2.38×10^{-4} ; FDR R-HSA-9006335 = 0.09; FDR R-HSA-8936459 = 0.03; R-HSA-76002 = 2.03×10^{-10} . (K) Enrichment ridge plots showing the distribution of enrichment scores in lung (red) and BM (blue) with individual cell placement on the rug plot to compare selected Gene Ontology Biological Process gene set enrichments. P values are given in the figure, FDR GO:00025 = 1.77×10^{-6} ; FDR GO:0001816 = 2.42×10^{-7} ; FDR GO:0006955 = 6.70×10^{-7} ; GO:0050729 = 2.02×10^{-8} . earlyEry, early erythroid progenitor; ECM, extracellular matrix; EMP, erythroid megakaryocytic progenitor; Eo/Ba/Ma, eosinophil/basophil/mast cell progenitor; FDR, false discovery rate; GFR, growth factor receptor; lateEry, late erythroid progenitor; MultiLin, multilineage; My, myeloid cell; nd, not determined; ns, not significant; prog/stroma mix, progenitor stroma cell mix.

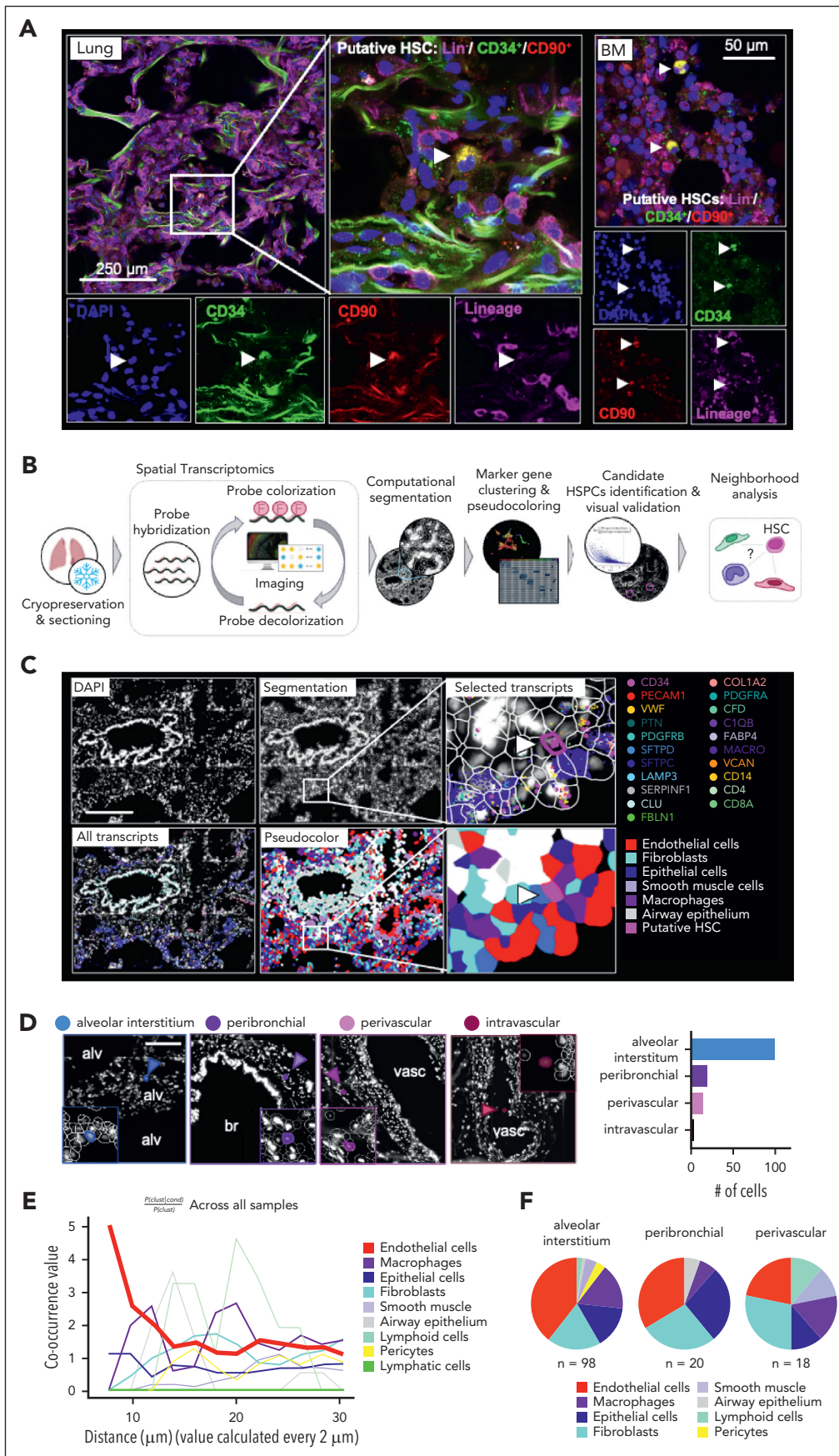


Figure 4.

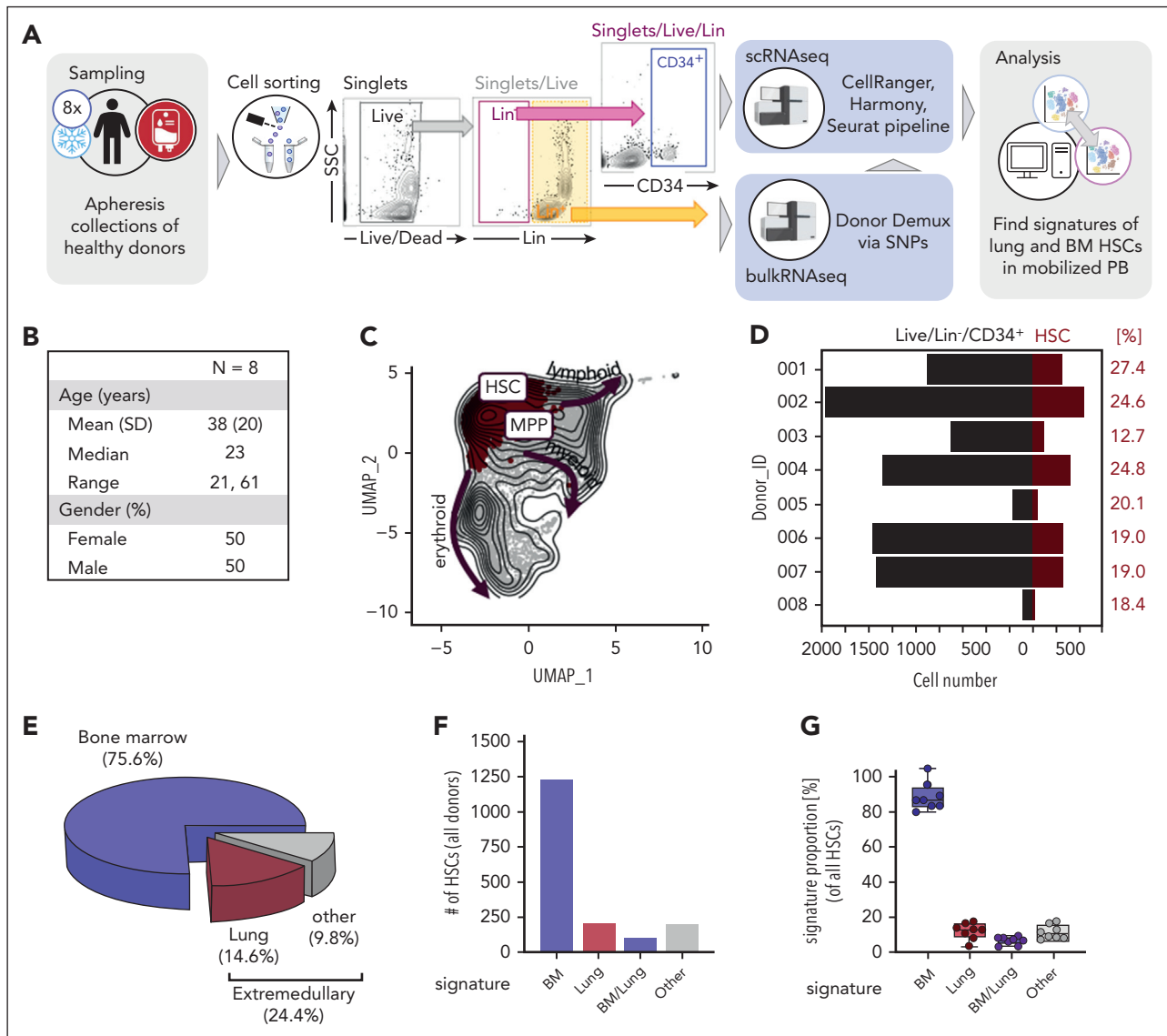


Figure 5. HSCs with pulmonary signatures are mobilized during apheresis collections for transplantation. (A) PB stem cells of 8 healthy donors given granulocyte colony-stimulating factor (G-CSF) for mobilization were collected via apheresis and cryopreserved (sampling). Live/Lin⁺/CD34⁺ cells were flow sorted and encapsulated; 10× Chromium Single 3' v2 libraries were prepared, pooled, and sequenced (scRNA-seq). For donor demultiplexing via single nucleotide polymorphisms, bulkRNAseq was performed on Live/Lin⁺ cells. After Louvain clustering and annotation, phenotypic HSCs were subsetted from the mobilized pool and examined for their expression of canonical, lung, and BM HSC signature genes using UCell. (B) Basic demographics of the donor population. (C) Batch-corrected UMAP representation highlighting the HSC/MPP cluster (red), arrows indicate developmental trajectory into more committed progenies (erythroid, myeloid, lymphoid). (D) The total number of progenitor cells and number of HSCs per donor. Fraction of HSCs among all cells is given in red. (E) Pie graph showing the proportions of medullary (blue) and extramedullary (lung, red; other, gray) signatures in the HSC fraction of apheresis samples. (F) Bar graph showing the absolute numbers of HSCs across all donor that had a unique BM (blue) or lung (red) signature, cells that exhibited features of both BM and lung (violet), and cells that could not be assigned to either of these categories (gray). (G) Box and whisker plot representing the percentage of medullary and extramedullary signatures identified the HSC population. Dots represent the individual allogeneic donors. bulkRNAseq, bulk RNA sequencing.

Figure 4. Spatial mapping of phenotypic CD34⁺ HSPCs in the lung. (A) Immunofluorescence imaging of putative HSCs (Lin⁻/CD34⁺/CD90⁺) in the human lung and BM. Left panel: representative section of lung showing a Lin⁻/CD34⁺/CD90⁺ in the interstitial space. Right panel: representative section of BM showing 2 Lin⁻/CD34⁺/CD90⁺ cells. (B) Spatial transcriptomics analysis workflow. smFISH was performed to visualize gene expression in human lung tissue. Transcripts were assigned to individual cells after cell segmentation and cells were annotated based on marker gene expression (supplemental Figure 10A-D). HSPC candidate cells were computationally identified based on their gene signature and visually validated (supplemental Figure 10E-F; supplemental Figure 11A-B). (C) Representative image of a putative HSPC in its pulmonary niche. Upper panel (left to right): DAPI staining, QuPath segmentation, zoom on putative HSPC (arrow). Selected transcripts are shown. Lower panel (left to right): all transcripts, pseudocoloring of cell types in the lung tissue based on marker clustering (supplemental Figure 10). Zoom on putative HSPC in niche. Scale bar, 250 μm. (D) Anatomic location of candidate cells in the lung. Representative images of phenotypic HSPCs in 4 major locations (alveolar interstitium, peribronchial, perivascular, or intravascular) and proportion of cells in each location. Scale bar, 150 μm. (E) Squidpy co-occurrence score computed every 2 μm between putative HSPCs and the rest of the clusters across lung tissue sections from 4 organ donors. High score values indicate greater co-occurrence probability; endothelial cells (red) co-occur with the HSPCs at short distances. (F) Pie graphs showing the proportion of neighboring cells within a radius of 20 μm from the putative HSPCs in the major anatomic locations. Alv, alveolar space; br, bronchus; DAPI, 4',6-diamidino-2-phenylindole; smFISH, single-molecule fluorescence in situ hybridization; vasc, vasculature.

variability in ischemia times during organ recovery, and differences in cell preparation methods for lung and BM affecting cell viability that could influence our results. Our studies rely heavily on transcriptomics and future studies will need to identify a lung HSC-specific marker to facilitate their identification. We have not addressed the ontogeny of lung HSPCs, something that is not possible given the restraints of our human tissue study. There is irrefutable evidence that HSCs commonly enter the circulation and microcirculatory beds, and given the functional and molecular similarities of lung HSPCs to other extramedullary HSPCs, this is perhaps the source of the tissue-resident HSPCs in the lung.^{36,44} However, there is precedence for tissue residency to be endowed during development, such as with yolk sac-derived macrophages.⁴⁵ Future studies will be needed to answer this question, including the possibility that hemogenic endothelium in the fetal lung could be the source.^{46,47} Our scRNA-seq analysis in blood stem cell donors provides important insights into the potential contribution of pulmonary HSCs to the mobilized blood progenitor pool, but these results need further validation. It is important to recognize that, owing to the limitations of direct methodologies in humans, our approach relies on organ-specific HSC signature scores to infer the tissue of origin.

Our findings reframe our understanding of the HSPC pool and its molecular diversity and should enable future studies that could potentially lead to therapeutic advances, such as for lifesaving HSC transplantation for BM malignancies and failure. In the modern era, transplantation is mainly accomplished using mobilized HSCs obtained from the PB. We have now shown that this pool is heterogeneous with a sizable extramedullary component that implies functional heterogeneity given our findings on lung HSC biases. These results have important implications for treatment responses and complications. Our findings may also help to understand the mechanisms of leukemogenesis with the possibility that lung HSPCs are direct targets of environmental carcinogens.⁴⁸ Furthermore, our findings add to our expanding understanding of rare cell types in the lung and their potential functions.⁴⁹

Acknowledgments

The authors thank Donor Network West, Michael Matthay (University of California San Francisco [UCSF]), and the Nina Ireland Program for Lung Health (UCSF) for providing human lung tissue from deceased organ donors.

This work was supported by an International Anesthesia Research Society (IARS) Mentored Research Award to C.C., the Deutsche Forschungsgemeinschaft Research Fellowships to C.C. (CO 2096/1-1) and N.M. (ME 5209/1-1), Bakar UCSF ImmunoX support to A.J.C., a Wellcome-Royal Society Sir Henry Dale Fellowship (107630/Z/15/Z) and funding in part by the Wellcome Trust [203151/Z/16/Z, 203151/A/16/Z] and the United Kingdom Research and Innovation (UKRI) Medical

Research Council [MC_PC_17230] to E.L., and National Institutes of Health (NIH), National Heart, Lung, and Blood Institute grant R35HL161241 to M.R.L. Sequencing was performed at the UCSF Center for Advanced Technology, supported by the UCSF Program for Breakthrough Biomedical Research, Research Resource Program Institutional Matching Instrumentation Award, and NIH, Office of the Director 1S10OD028511-01 grants.

Authorship

Contribution: C.C. designed and conducted experiments, analyzed the data, and wrote the manuscript; M.M. designed and conducted experiments; J.T., B.S., U.V., and A.J.C. assisted in designing and conducting experiments and helped analyzing the data; H.W. and M.N. helped analyzing the data; S.J.C., L.Q., J.J.T., and M.D.G. assisted in conducting experiments; A.D.L. provided human apheresis blood samples; E.P., E.L., and N.M. assisted in designing experiments, provided technical expertise with hematopoietic progenitor analyses, and provided editorial support on the manuscript; and M.R.L. designed the experiments, supervised the study, and wrote the manuscript.

Conflict-of-interest disclosure: The authors declare no competing financial interests.

ORCID profiles: C.C., 0000-0002-7160-9169; M.M., 0000-0001-5189-0072; J.T., 0000-0002-1336-6760; H.W., 0009-0007-5631-4067; M.N., 0000-0002-9025-2759; B.S., 0000-0002-2893-0897; S.J.C., 0000-0001-5573-6363; L.Q., 0000-0003-3122-9679; J.J.T., 0000-0002-3850-439X; N.M., 0000-0002-5078-2333; E.P., 0000-0002-3516-297X; E.L., 0000-0002-9917-9092; M.R.L., 0000-0003-0241-9190.

Correspondence: Mark R. Looney, Department of Medicine, University of California San Francisco, 513 Parnassus Ave, HSE 1355A, San Francisco, CA 94143-0130; email: mark.looney@ucsf.edu.

Footnotes

Submitted 4 December 2024; accepted 19 January 2025; prepublished online on *Blood* First Edition 27 February 2025. <https://doi.org/10.1182/blood.2024027884>.

Sequencing data have been deposited in the Gene Expression Omnibus database (accession code GSE255687).

There are no restrictions on data availability or use. The Human Lung Cell Atlas is publicly available data set that can be accessed at https://azimuth.hubmapconsortium.org/references/human_lung_v2/. Codes used in this study are available on request from the corresponding author, Mark R. Looney (mark.looney@ucsf.edu).

The online version of this article contains a data supplement.

There is a [Blood Commentary](#) on this article in this issue.

The publication costs of this article were defrayed in part by page charge payment. Therefore, and solely to indicate this fact, this article is hereby marked "advertisement" in accordance with 18 USC section 1734.

REFERENCES

- Weissman IL, Shizuru JA. The origins of the identification and isolation of hematopoietic stem cells, and their capability to induce donor-specific transplantation tolerance and treat autoimmune diseases. *Blood*. 2008; 112(9):3543-3553.
- Abkowitz JL, Catlin SN, McCallie MT, Guttorp P. Evidence that the number of hematopoietic stem cells per animal is conserved in mammals. *Blood*. 2002;100(7):2665-2667.
- Nombela-Arrieta C, Manz MG. Quantification and three-dimensional microanatomical organization of the bone marrow. *Blood Adv*. 2017;1(6):407-416.
- Wilkinson AC, Igarashi KJ, Nakauchi H. Haematopoietic stem cell self-renewal in vivo and ex vivo. *Nat Rev Genet*. 2020;21(9): 541-554.
- Verovskaya EV, Dellorusso PV, Passegue E. Losing sense of self and surroundings: hematopoietic stem cell aging and leukemic transformation. *Trends Mol Med*. 2019;25(6): 494-515.
- Jaiswal S, Ebert BL. Clonal hematopoiesis in human aging and disease. *Science*. 2019; 366(6465):eaan4673.
- Lefrançois E, Ortiz-Muñoz G, Caudrillier A, et al. The lung is a site of platelet biogenesis and a reservoir for hematopoietic progenitors. *Nature*. 2017;544(7648):105-109.

8. Belluschi S, Calderbank EF, Ciauro V, et al. Myelo-lymphoid lineage restriction occurs in the human haematopoietic stem cell compartment before lymphoid-primed multipotent progenitors. *Nat Commun*. 2018;9(1):4100.
9. Kang HM, Subramaniam M, Targ S, et al. Multiplexed droplet single-cell RNA-sequencing using natural genetic variation. *Nat Biotechnol*. 2018;36(1):89-94.
10. Notta F, Doulatov S, Laurenti E, Poepl A, Jurisica I, Dick JE. Isolation of single human hematopoietic stem cells capable of long-term multilineage engraftment. *Science*. 2011;333(6039):218-221.
11. Notta F, Zandi S, Takayama N, et al. Distinct routes of lineage development reshape the human blood hierarchy across ontogeny. *Science*. 2016;351(6269):aab2116.
12. Sanada C, Xavier-Ferrucio J, Lu YC, et al. Adult human megakaryocyte-erythroid progenitors are in the CD34+CD38mid fraction. *Blood*. 2016;128(7):923-933.
13. Green J, Endale M, Auer H, Perl AKT. Diversity of interstitial lung fibroblasts is regulated by platelet-derived growth factor receptor α kinase activity. *Am J Respir Cell Mol Biol*. 2016;54(4):532-545.
14. Nicolini FE, Cashman JD, Hogge DE, Humphries RK, Eaves CJ. NOD/SCID mice engineered to express human IL-3, GM-CSF and steel factor constitutively mobilize engrafted human progenitors and compromise human stem cell regeneration. *Leukemia*. 2004;18(2):341-347.
15. Park CY, Majeti R, Weissman IL. In vivo evaluation of human hematopoiesis through xenotransplantation of purified hematopoietic stem cells from umbilical cord blood. *Nat Protoc*. 2008;3(12):1932-1940.
16. McKenzie JL, Takenaka K, Gan OI, Doedens M, Dick JE. Low rhodamine 123 retention identifies long-term human hematopoietic stem cells within the Lin-CD34+CD38- population. *Blood*. 2007;109(2):543-545.
17. Goyama S, Wunderlich M, Mulloy JC. Xenograft models for normal and malignant stem cells. *Blood*. 2015;125(17):2630-2640.
18. Korsunsky I, Millard N, Fan J, et al. Fast, sensitive and accurate integration of single-cell data with harmony. *Nat Methods*. 2019;16(12):1289-1296.
19. Hay SB, Ferchen K, Chetal K, Grimes HL, Salomonis N. The Human Cell Atlas bone marrow single-cell interactive web portal. *Exp Hematol*. 2018;68:51-61.
20. Travaglini KJ, Nabhan AN, Penland L, et al. A molecular cell atlas of the human lung from single-cell RNA sequencing. *Nature*. 2020;587(7835):619-625.
21. Cao J, Spielmann M, Qiu X, et al. The single-cell transcriptional landscape of mammalian organogenesis. *Nature*. 2019;566(7745):496-502.
22. Sato A, Kamio N, Yokota A, et al. C/EBP β isoforms sequentially regulate regenerating mouse hematopoietic stem/progenitor cells. *Blood Adv*. 2020;4(14):3343-3356.
23. Mohanty JG, Nagababu E, Friedman JS, Rifkind JM. SOD2 deficiency in hematopoietic cells in mice results in reduced red blood cell deformability and increased heme degradation. *Exp Hematol*. 2013;41(3):316-321.
24. Barbosa CM, Bincoletto C, Barros CC, Ferreira AT, Paredes-Gamero EJ. PLC γ 2 and PKC are important to myeloid lineage commitment triggered by M-SCF and G-CSF. *J Cell Biochem*. 2014;115(1):42-51.
25. Kruta M, Sunshine MJ, Chua BA, et al. Hsf1 promotes hematopoietic stem cell fitness and proteostasis in response to ex vivo culture stress and aging. *Cell Stem Cell*. 2021;28(11):1950-1965.e6.
26. Livada AC, McGrath KE, Malloy MW, et al. Long-lived lung megakaryocytes contribute to platelet recovery in thrombocytopenia models. *J Clin Invest*. 2024;134(22):e181111.
27. Pariser DN, Hilt ZT, Ture SK, et al. Lung megakaryocytes are immune modulatory cells. *J Clin Invest*. 2021;131(1):e137377.
28. Sikkema L, Ramírez-Suástegui C, Strobl DC, et al. An integrated cell atlas of the lung in health and disease. *Nat Med*. 2023;29(6):1563-1577.
29. HuBMAP. Azimuth references. Accessed 24 October 2023. <https://azimuth.hubmapconsortium.org/references/#Human%20-%20Lung%20v2%20%28HLC%29>
30. Palla G, Spitzer H, Klein M, et al. Squidpy: a scalable framework for spatial omics analysis. *Nat Methods*. 2022;19(2):171-178.
31. Ghersi JJ, Baldissera G, Hintzen J, et al. Haematopoietic stem and progenitor cell heterogeneity is inherited from the embryonic endothelium. *Nat Cell Biol*. 2023;25(8):1135-1145.
32. Zhang Y, Liu F. The evolving views of hematopoiesis: from embryo to adulthood and from in vivo to in vitro. *J Genet Genomics*. 2024;51(1):3-15.
33. Mende N, Bastos HP, Santoro A, et al. Unique molecular and functional features of extramedullary hematopoietic stem and progenitor cell reservoirs in humans. *Blood*. 2022;139(23):3387-3401.
34. Spencer JA, Ferraro F, Roussakis E, et al. Direct measurement of local oxygen concentration in the bone marrow of live animals. *Nature*. 2014;508(7495):269-273.
35. Li D, Xue W, Li M, et al. VCAM-1(+) macrophages guide the homing of HSPCs to a vascular niche. *Nature*. 2018;564(7734):119-124.
36. Massberg S, Schaerli P, Knezevic-Maramica I, et al. Immunosurveillance by hematopoietic progenitor cells trafficking through blood, lymph, and peripheral tissues. *Cell*. 2007;131(5):994-1008.
37. Wright DE, Wagers AJ, Gulati AP, Johnson FL, Weissman IL. Physiological migration of hematopoietic stem and progenitor cells. *Science*. 2001;294(5548):1933-1936.
38. Acar M, Kocherlakota KS, Murphy MM, et al. Deep imaging of bone marrow shows non-dividing stem cells are mainly perisinusoidal. *Nature*. 2015;526(7571):126-130.
39. Kiel MJ, Yilmaz OH, Iwashita T, Yilmaz OH, Terhorst C, Morrison SJ. SLAM family receptors distinguish hematopoietic stem and progenitor cells and reveal endothelial niches for stem cells. *Cell*. 2005;121(7):1109-1121.
40. Cao Z, Lis R, Ginsberg M, et al. Targeting of the pulmonary capillary vascular niche promotes lung alveolar repair and ameliorates fibrosis. *Nat Med*. 2016;22(2):154-162.
41. Mammoto A, Mammoto T. Vascular niche in lung alveolar development, homeostasis, and regeneration. *Front Bioeng Biotechnol*. 2019;7:318.
42. Phan SH. Genesis of the myofibroblast in lung injury and fibrosis. *Proc Am Thorac Soc*. 2012;9(3):148-152.
43. Reilkoff RA, Bucala R, Herzog EL. Fibrocytes: emerging effector cells in chronic inflammation. *Nat Rev Immunol*. 2011;11(6):427-435.
44. Ceradini DJ, Kulkarni AR, Callaghan MJ, et al. Progenitor cell trafficking is regulated by hypoxic gradients through HIF-1 induction of SDF-1. *Nat Med*. 2004;10(8):858-864.
45. Gomez Perdiguero E, Klapproth K, Schulz C, et al. Tissue-resident macrophages originate from yolk-sac-derived erythro-myeloid progenitors. *Nature*. 2015;518(7540):547-551.
46. Yeung AK, Villacorta-Martin C, Lindstrom-Vautrin J, et al. De novo hematopoiesis from the fetal lung. *Blood Adv*. 2023;7(22):6898-6912.
47. Calvanese V, Capellera-Garcia S, Ma F, et al. Mapping human haematopoietic stem cells from haemogenic endothelium to birth. *Nature*. 2022;604(7906):534-540.
48. Zhao Y, Magaña LC, Cui H, et al. Formaldehyde-induced hematopoietic stem and progenitor cell toxicity in mouse lung and nose. *Arch Toxicol*. 2021;95(2):693-701.
49. Montoro DT, Haber AL, Biton M, et al. A revised airway epithelial hierarchy includes CFTR-expressing ionocytes. *Nature*. 2018;560(7718):319-324.

© 2025 American Society of Hematology. Published by Elsevier Inc. This is an open access article under the CC BY license (<http://creativecommons.org/licenses/by/4.0/>).